

Real-time observation of fluctuations at the driven-dissipative Dicke phase transition

Ferdinand Brennecke,¹ Rafael Mottl,¹ Kristian Baumann,^{1,2}
Renate Landig,¹ Tobias Donner,^{1,*} and Tilman Esslinger¹

¹*Institute for Quantum Electronics, ETH Zürich, CH-8093 Zürich, Switzerland*

²*present address: Departments of Applied Physics, Physics and E.L. Ginzton Laboratory, Stanford University, Stanford, California 94305, USA*

We experimentally study the influence of dissipation on the driven Dicke quantum phase transition, realized by coupling external degrees of freedom of a Bose-Einstein condensate to the light field of a high-finesse optical cavity. The cavity provides a natural dissipation channel, which gives rise to vacuum-induced fluctuations and allows us to observe density fluctuations of the gas in real-time. We monitor the divergence of these fluctuations over two orders of magnitude while approaching the phase transition and observe a behavior which significantly deviates from that expected for a closed system. A correlation analysis of the fluctuations reveals the diverging time scale of the atomic dynamics and allows us to extract a damping rate for the external degree of freedom of the atoms. We find good agreement with our theoretical model including both dissipation via the cavity field and via the atomic field. Utilizing a dissipation channel to non-destructively gain information about a quantum many-body system provides a unique path to study the physics of driven-dissipative systems.

Experimental progress in the creation, manipulation and probing of atomic quantum gases has made it possible to study highly controlled many-body systems and to access their phase transitions. This new approach to quantum many-body physics has substantiated the notion of quantum simulation for key models of condensed matter physics [1, 2]. There has been increasing interest in generalizing such an approach to zero-temperature or quantum phase transitions away from thermal equilibrium, as occurring in driven-dissipative systems [3–8]. Amongst the most tantalizing questions is how vacuum fluctuations from the environment influence the fluctuation spectrum at a phase transition via quantum backaction. Coupling quantum gases to the field of an optical cavity is a particularly promising approach to realize a driven-dissipative quantum many-body system with a well understood and controlled dissipation channel. A further advantage of this scheme is that the dissipation channel of the cavity mode can be directly used to investigate the system in a non-destructive way via the leaking cavity field [9].

Combining the experimental setting of cavity quantum electrodynamics with that of quantum gases [10–14] led to the observation of quantum backaction heating caused by cavity dissipation [15, 16], as well as to the realization of the non-equilibrium Dicke quantum phase transition [17]. Here, we study the influence of cavity dissipation on the fluctuation spectrum at the Dicke phase transition by connecting these approaches. We non-destructively observe diverging fluctuations of the order parameter when approaching the critical point, and find a distinct difference with respect to predictions for the closed, i.e. non-dissipative system.

In our experimental system, density wave excitations in a Bose-Einstein condensate (BEC) are coupled via a coherent laser field to the mode of a standing-wave op-

tical cavity. For strong enough coupling this causes a spatial self-organization of the atoms on a wavelength-periodic checkerboard pattern which is a realization of the driven-dissipative Dicke phase transition [17, 18]. The fluctuations triggering the phase transition are atomic density fluctuations. They are generated by long-range atom-atom interactions which are mediated by exchange of cavity photons [19]. In the presence of cavity decay, vacuum fluctuations enter the cavity, interfere with the coherent pump laser field, and drive the system to a steady state with increased density fluctuations [20, 21]. In turn, the cavity decay offers natural access to the system properties via the light field leaking out of the cavity, which allows us to measure the density fluctuations in real-time [9]. Except for the natural quantum backaction of this continuous measurement process [22], the system remains unperturbed by our observation.

SYSTEM DESCRIPTION

Hamiltonian dynamics

As described in our previous work [17, 19], we place a BEC of N atoms inside an ultrahigh-finesse optical cavity and pump the atoms transversally with a far-detuned standing-wave laser field (Fig. 1A). The closed-system dynamics is described by the Dicke model ([17, 18] and SI),

$$\hat{H} = \hbar\omega\hat{a}^\dagger\hat{a} + \hbar\omega_0\hat{J}_z + \frac{2\hbar\lambda}{\sqrt{N}}(\hat{a} + \hat{a}^\dagger)\hat{J}_x, \quad (1)$$

where ω denotes the detuning between pump laser frequency ω_p and dispersively shifted cavity resonance frequency ω_c , and \hbar is Planck's constant divided by 2π . The annihilation operator of a cavity photon in a frame rotat-

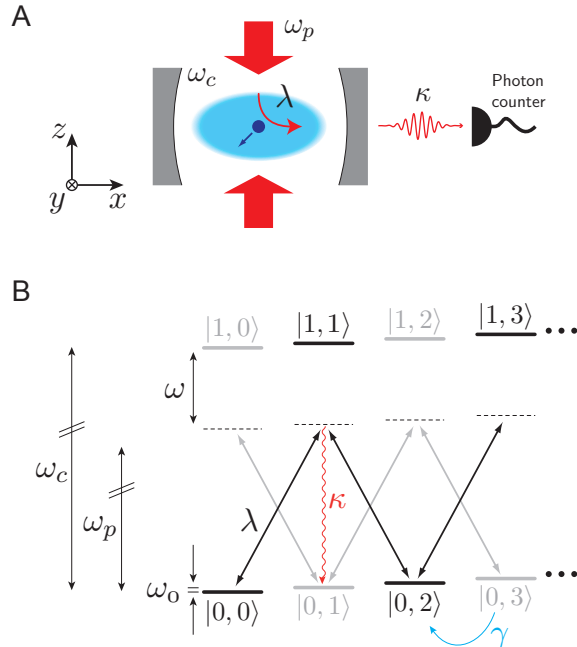


FIG. 1: **A.** Experimental scheme: A transverse pump field (red) couples an excited momentum mode of a BEC (blue) to a cavity mode via collective light scattering at rate λ . The cavity provides a loss channel for the system through which photons can escape. Density fluctuations are inferred from the detected cavity output field. **B.** Level scheme of the system after elimination of the electronically excited atomic states. The ground state of the closed coupled system is given by a coherent superposition of states $|n_a, n_b\rangle$ with even parity (black symbols). Here, n_a is the number of intracavity photons and n_b is the number of momentum excitations. Decay processes drive the system to a steady state which also includes an incoherent population of states with odd parity (grey symbols), caused by either the decay of a cavity photon at rate 2κ or the decay of a momentum excitation at rate 2γ . The depicted level scheme is restricted to $n_a \leq 1$.

ing at ω_p is given by \hat{a} . The atomic dynamics is captured in a two-mode description, consisting of the macroscopically populated zero-momentum mode ψ_0 of the BEC, and an excited momentum mode ψ_1 , carrying in a symmetric superposition one photon momentum along the $\pm x$ direction and one along the $\pm z$ direction. This defines an effective two-level system with energy splitting $\hbar\omega_0 = \hbar^2 k^2/m$, where k denotes the optical wavevector and m the atomic mass. The atomic ensemble of N such two-level systems can be described by collective spin operators \hat{J}_x , \hat{J}_y and \hat{J}_z . The expectation value $\langle \hat{J}_x \rangle$ measures the checkerboard density modulation which results from the interference between coherent populations of the two matter wave modes and can be identified as order parameter of the phase transition. The coupling

strength $\lambda \propto \sqrt{P}$ between atomic motion and light field can be experimentally controlled via the power P of the transverse pump field, and represents the collective two-photon Rabi frequency of the underlying scattering process between pump and cavity field (Fig. 1A). When λ reaches the critical coupling strength $\lambda_{\text{cr}} = \frac{\sqrt{\omega\omega_0}}{2}$, Hamiltonian (1) gives rise to a second-order quantum phase transition [23] towards a phase characterized by a non-zero order parameter $\langle \hat{J}_x \rangle \neq 0$, and a coherent cavity field, $\langle \hat{a} \rangle \neq 0$. Below the critical point, the system is in the normal phase, $\langle \hat{J}_x \rangle = \langle \hat{a} \rangle = 0$, where only fluctuations of the order parameter, $\langle \hat{J}_x^2 \rangle \neq 0$, give rise to an incoherent cavity field with $\langle \hat{a}^\dagger \hat{a} \rangle \neq 0$.

In the thermodynamic limit, the fluctuations of the order parameter in the normal phase can be described with bosonic creation and annihilation operators \hat{b}^\dagger and \hat{b} according to $J_x = \sqrt{N}(\hat{b} + \hat{b}^\dagger)/2$ (SI). The interaction term in Eq. (1) then becomes $\hbar\lambda(\hat{a} + \hat{a}^\dagger)(\hat{b} + \hat{b}^\dagger)$, and couples the bare states $|n_a, n_b\rangle$ under parity conservation of the total number of excitations $n_a + n_b$. Here, n_a is the number of photons stored in the cavity and n_b is the number of excitations in the momentum mode ψ_1 (Fig. 1). The ground state of the closed, coupled system is a two-mode squeezed state [24, 25] with admixtures of the even parity states only ($|0,0\rangle, |1,1\rangle, |0,2\rangle, \dots$). For $\omega \gg \omega_0$, the cavity is almost only virtually populated, i.e. the admixture of states with $n_a \neq 0$ is suppressed by ω_0/ω . The quantum fluctuations of the Hamiltonian system then correspond dominantly to pairs of atoms in the excited momentum mode ψ_1 . They are created and annihilated by quasi-resonant scattering of a pump photon into the cavity mode and back into the pump field at a rate $\frac{\lambda^2}{\omega}$. Towards λ_{cr} , the variance $\langle (\hat{b} + \hat{b}^\dagger)^2 \rangle$ of the resulting density fluctuations diverges, while the gas still does not show a density modulation ($\langle \hat{b} + \hat{b}^\dagger \rangle = 0$).

Dissipative dynamics

In the case of the open system, the tiny population of states with $n_a \neq 0$ becomes important. As this decays via cavity dissipation, the ladder of states with odd parity ($|1,0\rangle, |0,1\rangle, |1,2\rangle, |0,3\rangle, \dots$) is incoherently populated (Fig. 1). The microscopic process corresponds to the loss of a cavity photon at one of the mirrors before the coherent scattering back into the pump beam can be completed. The system will thus leave its ground state and irreversibly evolve into a non-equilibrium steady state with additional density fluctuations and a constant energy flow from the pump laser to the cavity output. The variance of the resulting incoherent cavity population $\langle \hat{a}^\dagger \hat{a} \rangle$ has been predicted to diverge at λ_{cr} with a critical exponent of 1.0 compared to the closed system exponent of 0.5 [20, 21]. The depletion of the ground state takes place at rate $\kappa_{\text{eff}} = \frac{\lambda^2}{\omega^2 + \kappa^2} \cdot \kappa$, where κ is the decay rate

of the cavity field [18]. In the experiment, κ_{eff} can be tuned and we choose $\omega \approx 8\kappa$, such that the rate of decay processes is almost an order of magnitude below the long-range interaction rate λ^2/ω .

The observable in our experiment is light leaking out of the cavity. Since for $\kappa \gg \omega_0$ the cavity field adiabatically follows the atomic motion, the cavity output field provides a sensitive tool to monitor the order parameter and its fluctuations in real time (SI, [9]). Checkerboard density fluctuations with variance $\langle (\hat{b} + \hat{b}^\dagger)^2 \rangle$ induce a finite incoherent population of the cavity field according to $\langle \hat{a}^\dagger \hat{a} \rangle = \frac{1}{4} \frac{\omega_0}{\omega} \left(\frac{\lambda}{\lambda_{\text{cr}}} \right)^2 \langle (\hat{b} + \hat{b}^\dagger)^2 \rangle$. Cavity decay amounts to a continuous measurement of the intracavity light field and causes, due to inherent matter-light entanglement, a quantum backaction upon the atomic system [22]. The role of the photons leaking out of the cavity is thus two-fold: they drive the system to a steady state of enhanced fluctuations and reveal real-time information about the total density fluctuations.

RESULTS

Data acquisition

Using this concept, we experimentally observe density fluctuations of the atomic ensemble in the normal phase while approaching the phase transition. We prepare the system with $N = 1.6(2) \cdot 10^5$ ^{87}Rb atoms at an intermediate coupling of $(\lambda/\lambda_{\text{cr}})^2 \approx 0.55$ and at a detuning of $\omega = 2\pi \cdot 10.0(5)$ MHz. Then, the transverse pump-laser power is linearly increased within a data acquisition time of 0.8 s to a value slightly beyond the critical point. For our parameters, $\omega_0 = 2\pi \cdot 8.3(2)$ kHz and $\kappa = 2\pi \cdot 1.25(5)$ MHz [19], the rate κ_{eff} at which the steady state is approached is $2\pi \cdot 1$ kHz for $\lambda = \lambda_{\text{cr}}$ [18]. We can therefore assume the system to be in steady state throughout the measurement. The inset in Fig. 2 displays the data of a single experimental run, where we monitor the stream of photons leaking out of the cavity with a single-photon counting module. From the photon count rate r we deduce the intracavity photon number $\bar{n} = (r - r_b)/2\kappa\eta$, taking into account the measured total detection efficiency of $\eta = 5(1)\%$ and the independently calibrated background count rate r_b . We observe a progressively increasing photon count rate with increasing transverse pump laser power, until a steep rise marks the transition point to the ordered phase. The exact position of the transition depends on the total number of atoms which fluctuates by 10% between repeated experimental runs. Therefore, we define a threshold for the count rate to detect the transition point (SI). This allows us to convert the time axis into linearly increasing coupling.

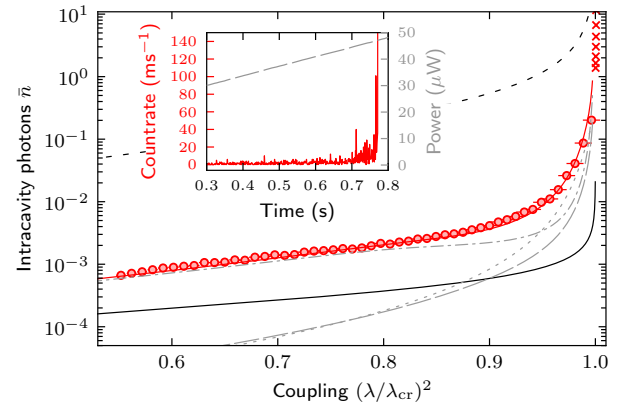


FIG. 2: Mean intracavity photon number \bar{n} (red symbols) as a function of coupling. Circles (crosses) indicate data in the normal (ordered) phase, the errorbars display the statistical error. The calculated expectations for the closed system are shown as solid black line. Our open-system description (solid red line) includes cavity field fluctuations due to the decay of photons and momentum excitations (grey dashed-dotted line) and due to the finite temperature of the BEC (grey dashed line), as well as a symmetry breaking coherent cavity field (grey dotted line). We also show the calculated fluctuations if the atomic damping rate γ would vanish (black dashed line). **Inset:** The raw data of a single run (red line) is displayed together with the measured transverse pump power (grey dashed line) as a function of time. The sudden increase in the photon count rate clearly marks the transition point.

Mean intracavity photon number

We average the signal of 372 experimental runs and observe the divergence of the intracavity photon number \bar{n} over three orders of magnitude, ending in a steep increase after passing the critical point (Fig. 2). We compared the measured intracavity photon number with the cavity field fluctuations expected from the ground state of the closed system [24]. Our data clearly shows an enhanced cavity field occupation with respect to the Hamiltonian system (solid black line in Fig. 2). This is in accordance with the presented picture that cavity decay increases fluctuations. Yet, the magnitude of the observed fluctuations is well below the theoretical expectation [20, 21] for a cavity decay at rate κ (dashed black line in Fig. 2). This indicates the presence of a further dissipation channel which damps out atomic momentum excitations.

Correlation analysis

Additional insight into the fluctuation dynamics and possible dissipative processes can be gained from a correlation analysis of the cavity output field. We calculate

the second-order correlation function for all experimental data contributing to Fig. 2. Since the cavity field adiabatically follows the atomic dynamics, its second-order correlation function $g^{(2)}(\tau) \propto \langle \hat{a}^\dagger(\tau) \hat{a}^\dagger(0) \hat{a}(0) \hat{a}(\tau) \rangle$ is linked to the temporal correlation function of the order parameter fluctuations $\langle \hat{J}_x^2(\tau) \hat{J}_x^2(0) \rangle$. The evaluated correlations as a function of time and coupling are shown in Fig. 3, together with cuts for specific coupling values. In contrast to a purely coherent cavity output field, which would yield a flat correlation function, we observe enhanced correlations for short times, followed by damped oscillations. The frequency of these oscillations agrees with the excitation energy of the coupled system, $\hbar\omega_s = \hbar\omega_0\sqrt{1 - (\lambda/\lambda_{cr})^2}$, which softens with increasing coupling and tends towards zero at the critical point. This shows that the cavity output field indeed carries information about the incoherent fluctuations of the system, and is consistent with our previous measurement of a mode softening and a diverging response [19]. A vanishing excitation frequency corresponds to a critical slowing down of the dynamics. Within our measurement resolution, however, the system adiabatically follows the steady state since the rate of change $d/dt(\lambda/\lambda_{cr})^2$ is only a few Hz [26].

We attribute the damping of the oscillations in $g^{(2)}(\tau)$ to the decay of atomic momentum excitations. This constitutes an additional dissipation channel caused by collisional and possibly cavity-mediated coupling of momentum excitations to Bogoliubov modes of the BEC [27, 28]. The observed decay rate of $g^{(2)}(\tau)$ cannot be explained by a finite admixture of the cavity field in the steady state, since ω exceeds ω_0 by orders of magnitude in our system [20].

The oscillations in the second-order correlation function exhibit an overperiod which becomes more pronounced towards the critical point. This indicates the presence of a finite coherent cavity field amplitude $\alpha = \langle \hat{a} \rangle$ which we attribute to the finite cloud size of the BEC and residual scattering of pump light at the edges of the cavity mirrors [17]. Interference between the coherent and incoherent cavity field components then causes the observed overperiod in the correlation function.

Quantum Langevin description

To quantitatively describe our observations, we developed a theoretical model based on coupled quantum Langevin equations [29] capturing the dynamics of the driven-dissipative system (SI). Our model explicitly takes into account the dissipation of the cavity field at rate κ , and furthermore a dissipation channel for excitations in the atomic momentum mode ψ_1 . For simplicity, this dissipation channel is phenomenologically modeled by a thermal Markovian bath at the BEC temperature of 100(20) nK into which excitations in the momentum

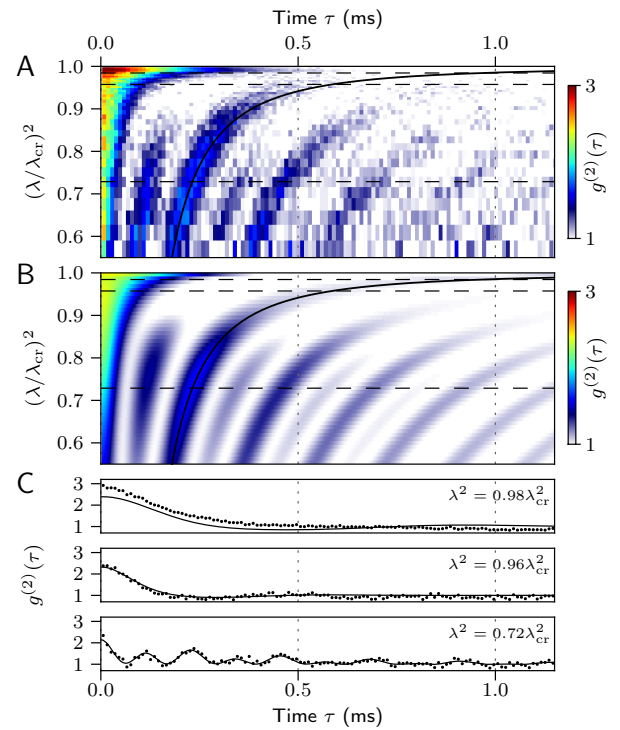


FIG. 3: Temporal correlations of the cavity output. Panel **A** shows a color plot of the measured second-order correlation function $g^{(2)}(\tau)$ as a function of time τ and coupling $(\lambda/\lambda_{cr})^2$. The correlation time increases with increasing coupling in agreement with the timescale related to the lowest excitation energy ω_s of the coupled system (solid black line). Panel **B** shows the correlations $g^{(2)}(\tau)$ calculated from the full theoretical model with parameters ζ and γ adjusted to match the data. The horizontal dashed lines indicate values of $(\lambda/\lambda_{cr})^2$ along which the data is shown (points) on the lower three panels **C** together with the full theory.

mode ψ_1 decay at a rate γ (SI). Due to the softening excitation frequency ω_s , the decay rate γ is taken as a function of the coupling rate λ . Our model further includes a small symmetry breaking field, which results in a coherent cavity field amplitude α already below the critical point. This is taken into account by renormalizing the order parameter with a constant offset ζ in Eq. (1) [17].

From the solution of the quantum Langevin equations in the thermodynamic limit we obtain the second-order correlation function of the intracavity field in the steady state (SI). The free parameters of our model description (ζ and γ) are extracted from fits of the model to the correlation data (Fig. 3). We obtain an order parameter offset $\zeta = 60(7)$ at $\lambda = 0$, which corresponds to 0.8% of the maximal possible order parameter $N/2$. This agrees with our earlier investigation of the symmetry breaking

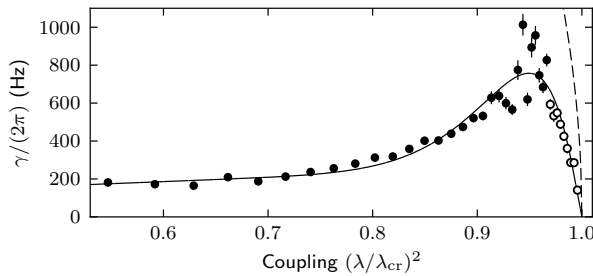


FIG. 4: Damping rate γ (symbols) as a function of coupling $(\lambda/\lambda_{\text{cr}})^2$ deduced from the cavity output correlation data. Errorbars indicate the statistical error derived from the fit. Open circles indicate the region above $(\lambda/\lambda_{\text{cr}})^2 = 0.97$, where our theoretical model deviates significantly from the data and values for γ might be inaccurate. The solid line shows the phenomenological function used to model the data in Fig. 2A. The dashed line shows the vanishing excitation frequency $\omega_s/2\pi$ of the system.

field [26].

The extracted damping rate γ is displayed in Fig. 4 as a function of coupling. It increases with increasing coupling, until it exhibits a cusp around 95% of the critical coupling and vanishes towards the critical point. We attribute this behavior mainly to the softening of the excitation frequency ω_s (dashed line in Fig. 4, [19]) which influences the density of states into which the momentum excitations in mode ψ_1 can decay. At the critical point, this is expected to lead to the absence of damping of the excited momentum mode [27, 30].

Our model describes our data very well for coupling values up to $(\lambda/\lambda_{\text{cr}})^2 \simeq 0.97$. Above this value, we observe enhanced correlations for small τ which are not captured by the model, as can be seen in the uppermost subpanel of Fig. 3C. We believe that in this region technical fluctuations, the dynamical change in the dispersive cavity shift [31], finite- N effects [32], and population of higher order momentum states start to play a role.

Using the extracted atomic damping rate and symmetry breaking field magnitude, we find very good agreement between the observed intracavity photon number and our model (Fig. 2). The inclusion of atomic damping is crucial for the quantitative description. While cavity decay is expected to lead to a strong increase of the density fluctuations, atomic dissipation dominantly damps out these momentum excitations, such that the total fluctuations in the steady state are only moderately enhanced with respect to the ground state fluctuations. Except for a small region close to the critical point, the dominant contribution to the observed fluctuations originates from vacuum input noise associated with dissipation via the cavity (grey dashed-dotted line in Fig. 2). Only close to the critical point, fluctuations from the

thermal atomic bath are predicted to contribute because the energy of the relevant mechanical excitation vanishes towards the phase transition [19].

Density fluctuations

We infer the variance of the density fluctuations $\langle (\hat{b} + \hat{b}^\dagger)^2 \rangle$ in the normal phase by rescaling the intracavity photon number \bar{n} after subtracting the coherent fraction $|\alpha|^2$, which was deduced from the correlation analysis (Fig. 5). Due to the uncertainties in the symmetry breaking field ζ , this procedure results in systematical uncertainties of the deduced density fluctuations which are reflected in the presented error bars. Our data, displayed on a log-log scale, deviates clearly in both magnitude and scaling from the expectations for the closed system. A linear fit (blue line) to the data results in an exponent of $0.9(\pm 0.1)$. Scaling with exponent 1.0 was predicted from open-system calculations in which only cavity dissipation is taken into account [20, 21]. The influence of the additional atomic dissipation rate γ on the scaling of the atomic density fluctuations depends on the precise scaling of this damping rate when approaching the critical point, which goes beyond the scope of this publication.

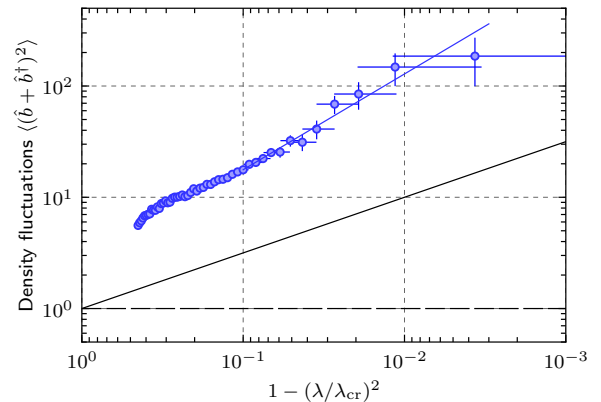


FIG. 5: Variance of the checkerboard density fluctuations of the BEC, deduced from the intracavity photon number after subtracting the coherent contribution. For comparison, we show the theory of the closed system (black line) which diverges with a critical exponent of 0.5, and a linear fit (blue line) to the data for $(\lambda/\lambda_{\text{cr}})^2 \geq 0.9$ that results in an exponent of 0.9 ± 0.1 . We also plot the expected fluctuations for a BEC without coupling to the cavity field (black dashed line). The horizontal errorbars indicate the statistical error, while the vertical errorbars result from the uncertainty in the subtracted coherent field component (SI).

DISCUSSION

From a more general perspective, driven systems, coupled via a dissipation channel to a zero-temperature Markovian bath, are expected to resemble classical critical behavior and can then be characterized in steady state by an effective temperature which depends on the considered observable [3–6, 33]. In our system, the zero-temperature bath is provided by the optical vacuum modes outside the cavity. Verifying the fluctuation-dissipation theorem for the order parameter in our system would allow to determine its effective temperature. The theoretical expectation of a critical exponent of 1.0 [20, 21] is a further indication that systems undergoing a driven-dissipative phase transition can be described to be effectively thermalized. However, answering the question whether cavity dissipation completely destroys the quantum character of the system, e.g. the entanglement between atomic and light fields, remains a challenge for future experiments [20, 29].

CONCLUSION AND OUTLOOK

We have demonstrated the direct observation of diverging density fluctuations in a quantum gas undergoing the driven-dissipative Dicke phase transition. This experiment opens a route to study quantum phase transitions in open systems under well controlled conditions. Our method directly uses the cavity dissipation channel to obtain real-time information on the fluctuations of the order parameter. In a similar way, intriguing quantum many-body states with long-range atom-atom interactions and the influence of dissipation on them can be investigated e.g. by using multi-mode cavities which allow to realize glassy and frustrated states of matter [33, 34]. Adding classical optical lattices to the system would let the energy scale of contact interactions enter the dynamics and should allow the exploration of rich phase diagrams [35, 36].

ACKNOWLEDGEMENTS

We acknowledge insightful discussions with I. Carusotto, S. Diehl, P. Domokos, S. Gopalakrishnan, S. Huber, A. Imamoglu, M. Paternostro, C. Rama, H. Ritsch, G. Szirmai, and H. Türeci. Supported by Synthetic Quantum Many-Body Systems (European Research Council advanced grant), Nanodesigning of Atomic and Molecular Quantum Matter (European Union, Future and Emerging Technologies open), National Centre of Competence in Research/Quantum Science and Technology, and the European Science Foundation (POLATOM).

* Email: donner@phys.ethz.ch

- [1] Bloch I, Dalibard J, Zwerger W (2008) Many-body physics with ultracold gases. *Reviews of Modern Physics* **80**, 885964.
- [2] Lewenstein M, Sanpera A, Ahufinger V. (2012) *Ultracold Atoms in Optical Lattices: Simulating quantum many-body systems*. (Oxford University Press).
- [3] Mitra A, Takei S, Kim Y, Millis A (2006) Nonequilibrium Quantum Criticality in Open Electronic Systems. *Physical Review Letters* **97**, 236808.
- [4] Diehl S, Micheli A, Kantian A, Kraus B, Büchler H. P, Zoller P (2008) Quantum states and phases in driven open quantum systems with cold atoms. *Nature Physics* **4**, 878–883.
- [5] Dalla Torre E. G, Demler E, Giamarchi T, Altman E (2010) Quantum critical states and phase transitions in the presence of non-equilibrium noise. *Nature Physics* **6**, 806–810.
- [6] Torre E. G. D, Diehl S, Lukin M. D, Sachdev S, Strack P (2012) Keldysh approach for nonequilibrium phase transitions in quantum optics: Beyond the Dicke model in optical cavities. *Physical Review A* **87**, 023831.
- [7] Sieberer L. M, Huber S. D, Altman E, Diehl S (2013) Dynamical critical phenomena in driven-dissipative systems. *arXiv* 1301.5854.
- [8] Kessler E, Giedke G, Imamoglu A, Yelin S, Lukin M, Cirac J (2012) Dissipative phase transition in a central spin system. *Physical Review A* **86**, 012116.
- [9] Mekhov I. B, Maschler C, Ritsch H (2007) Probing quantum phases of ultracold atoms in optical lattices by transmission spectra in cavity quantum electrodynamics. *Nature Physics* **3**, 319–323.
- [10] Brennecke F, Donner T, Ritter S, Bourdel T, Köhl M, Esslinger T (2007) Cavity QED with a Bose-Einstein condensate. *Nature* **450**, 268–71.
- [11] Colombe Y, Steinmetz T, Dubois G, Linke F, Hunger D, Reichel J (2007) Strong atom-field coupling for Bose-Einstein condensates in an optical cavity on a chip. *Nature* **450**, 272–6.
- [12] Gupta S, Moore K, Murch K, Stamper-Kurn D (2007) Cavity Nonlinear Optics at Low Photon Numbers from Collective Atomic Motion. *Physical Review Letters* **99**, 213601.
- [13] Wolke M, Klinner J, Kessler H, Hemmerich A (2012) Cavity cooling below the recoil limit. *Science* **337**, 75–8.
- [14] Ritsch H, Domokos P, Brennecke F, Esslinger T (2013) Cold atoms in cavity-generated dynamical optical potentials. *Review of Modern Physics* **85**, 553–601.
- [15] Murch K. W, Moore K. L, Gupta S, Stamper-Kurn D. M (2008) Observation of quantum-measurement backaction with an ultracold atomic gas. *Nature Physics* **4**, 561–564.
- [16] Brahms N, Botter T, Schreppler S, Brooks DWC, Stamper-Kurn DM (2012) Optical detection of the quantization of collective atomic motion *Physical Review Letters* **108**, 133601.
- [17] Baumann K, Guerlin C, Brennecke F, Esslinger T (2010) Dicke quantum phase transition with a superfluid gas in an optical cavity. *Nature* **464**, 1301–1306.
- [18] Nagy D, Kónya G, Szirmai G, Domokos P (2010) Dicke-Model Phase Transition in the Quantum Motion of a Bose-Einstein Condensate in an Optical Cavity. *Phys-*

- ical Review Letters **104**, 130401.
- [19] Mottl R, Brennecke F, Baumann K, Landig R, Donner T, Esslinger T (2012) Roton-type mode softening in a quantum gas with cavity-mediated long-range interactions. *Science* **336**, 1570–3.
- [20] Nagy D, Szirmai G, Domokos P (2011) Critical exponent of a quantum-noise-driven phase transition: The open-system Dicke model. *Physical Review A* **84**, 043637.
- [21] Öztürk B, Bordyuh M, Müstecaplolu O. E, Türeci H. E (2012) Excitations of optically driven atomic condensate in a cavity: theory of photodetection measurements. *New Journal of Physics* **14**, 085011.
- [22] Braginsky V. B, Khalili F. Y, Thorne K. S. (1993) *Quantum measurement*. (Cambridge University Press) Vol. 32.
- [23] Emery C, Brandes T (2003) Quantum Chaos Triggered by Precursors of a Quantum Phase Transition: The Dicke Model. *Physical Review Letters* **90**, 044101.
- [24] Emery C, Brandes T (2003) Chaos and the quantum phase transition in the Dicke model. *Physical Review E* **67**, 066203.
- [25] Milburn G. J, Walls D. F. (2008) *Quantum Optics*. (Springer).
- [26] Baumann K, Mottl R, Brennecke F, Esslinger T (2011) Exploring Symmetry Breaking at the Dicke Quantum Phase Transition. *Physical Review Letters* **107**, 140402.
- [27] Graham R (2000) Langevin equation of collective modes of Bose-Einstein condensates in traps. *Journal of Statistical Physics* **101**, 243–257.
- [28] Katz N, Steinhauer J, Ozeri R, Davidson N (2002) Beliaev Damping of Quasiparticles in a Bose-Einstein Condensate. *Physical Review Letters* **89**, 220401.
- [29] Dimer F, Estienne B, Parkins A, Carmichael H (2007) Proposed realization of the Dicke-model quantum phase transition in an optical cavity QED system. *Physical Review A* **75**, 013804.
- [30] private communication with G. Szirmai and P. Domokos.
- [31] Keeling J, Bhaseen M, Simons B (2010) Collective Dynamics of Bose-Einstein Condensates in Optical Cavities. *Physical Review Letters* **105**, 043001.
- [32] Kónya G, Szirmai G, Domokos P (2011) Multimode mean-field model for the quantum phase transition of a Bose-Einstein condensate in an optical resonator. *The European Physical Journal D* **65**, 33–42.
- [33] Gopalakrishnan S, Lev B. L, Goldbart P. M (2009) Emergent crystallinity and frustration with Bose-Einstein condensates in multimode cavities. *Nature Physics* **5**, 845–850.
- [34] Strack P, Sachdev S (2011) Dicke Quantum Spin Glass of Atoms and Photons. *Physical Review Letters* **107**, 277202.
- [35] Larson J, Damski B, Morigi G, Lewenstein M (2008) Mott-Insulator States of Ultracold Atoms in Optical Resonators. *Physical Review Letters* **100**, 050401.
- [36] Habibian H, Winter A, Paganelli S, Rieger H, Morigi G (2013) Bose-glass phases of ultracold atoms due to cavity backaction. *Physical Review Letters* **110**, 075304.

Supplementary Information

Experimental details and data analysis

The experimental sequence for the measurements presented is as follows. After preparing an almost pure Bose-Einstein condensate in a crossed-beam dipole trap which is centered with respect to the TEM₀₀ cavity mode, the transverse pump power P is increased over 50 ms to a relative coupling strength of $\lambda^2/\lambda_{\text{cr}}^2 \approx 0.55$. Subsequently, the power P is linearly increased over 0.8 s to slightly beyond the critical pump power, while the stream of photons leaking out of the cavity is recorded on a single-photon counting module. Intracavity photons are detected with an efficiency of 5%, limited mainly by the losses in the cavity mirrors and the detection efficiency of the single-photon counter. We carefully calibrated the background count rate of the photon detector in the absence of atoms yielding a maximum rate of 341(62)/s. This results from dark counts (at a rate of 100(10)/s) and stray light of the transverse pump beam and the dipole trap beams. The background signal is subtracted from the overall count rate recorded in the presence of atoms to obtain the mean intracavity photon number, as shown in Figure 2.

A steep increase of the photon count rate indicates the phase transition point and allows to convert the recording time axis into a relative coupling axis $\lambda^2/\lambda_{\text{cr}}^2$. To this end we identify the timebin of 100 μs length in which the photon count rate exceeds for the first time the value of $18 \mu\text{s}^{-1}$ corresponding to a mean intracavity photon number of approximately 49. According to the typical risetime of the intracavity signal, the critical point is defined as the time 1 ms prior to this timebin. The relative error of λ_{cr} according to this procedure is given by $5 \cdot 10^{-4}$. Residual atom loss of 10% during probing is taken into account by rescaling the relative coupling axis according to the proportionality $P_{\text{cr}} \propto N^{-1}$. This is justified by the resulting match between the oscillation frequency of the second-order correlation function and the softening excitation frequency, which was measured independently in [S1].

For the correlation analysis, the recorded photon data is cut into subtraces whose length decreases to a minimal value of 4 ms as the critical point is approached. For each subtrace the photon-photon correlation function is computed (using time bins of 2 μs). The normalized correlation functions are finally averaged over all 372 experimental runs.

The temperature of the initially prepared Bose-Einstein condensate was determined from absorption images to

$T = 65(20)$ nK. During probing, this value is expected to increase by 35 nK due to spontaneous emission and decay of atomic momentum excitations into the bath of Bogoliubov modes (see below). Further experimental details can be found in [S1, S2].

Theoretical model

Two-mode description and Dicke model

We model the dynamics of the transversally driven BEC-cavity system in a two-mode description which formally is equivalent to the Dicke Hamiltonian, as was shown previously [S2, S3]. The relevant motional states which are coupled via two-photon transitions between pump and cavity fields are given by the macroscopically populated condensate mode ψ_0 and the motionally excited mode ψ_1 which carries in a coherent superposition momenta $(p_x, p_z) = (\pm\hbar k, \pm\hbar k)$ along the cavity (x) and pump (z) directions. To first order, these matter wave modes are separated in energy by $\hbar\omega_0 = 2\hbar\omega_R$, with recoil frequency $\omega_R = \hbar k^2/2m$, optical wavevector $k = 2\pi/\lambda$ and atomic mass m . Atomic s-wave scattering and a weak $\lambda/2$ -periodic lattice potential caused by the transverse pump field induce a small shift of $\hbar\omega_0$ [S1].

After expanding the atomic field operator in this two-mode basis, $\hat{\Psi} = \hat{c}_0\psi_0 + \hat{c}_1\psi_1$, and introducing corresponding collective spin- $N/2$ operators (where N denotes the total number of atoms)

$$\hat{\mathbf{J}} = \begin{pmatrix} \hat{J}_x \\ \hat{J}_y \\ \hat{J}_z \end{pmatrix} = \begin{pmatrix} \frac{1}{2}(\hat{c}_1^\dagger\hat{c}_0 + \hat{c}_0^\dagger\hat{c}_1) \\ \frac{1}{2i}(\hat{c}_1^\dagger\hat{c}_0 - \hat{c}_0^\dagger\hat{c}_1) \\ \frac{1}{2}(\hat{c}_1^\dagger\hat{c}_1 - \hat{c}_0^\dagger\hat{c}_0) \end{pmatrix}, \quad (2)$$

the many-body Hamiltonian of the BEC-cavity system is given by the Dicke Hamiltonian

$$\hat{H}/\hbar = \omega\hat{a}^\dagger\hat{a} + \omega_0\hat{J}_z + 2\lambda/\sqrt{N}(\hat{a} + \hat{a}^\dagger)\hat{J}_x. \quad (3)$$

Note that the time-dependence of the driven system was formally eliminated by moving into a reference frame rotating at the pump laser frequency ω_p . In equation (3), \hat{a} annihilates a photon in the cavity mode with resonance frequency ω_c , which in the experiment is blue-detuned from the pump laser frequency ω_p by the amount $\omega = \omega_c - \omega_p = 2\pi \times 10$ MHz. Here, the dispersive cavity shift caused by the bare condensate ($2\pi \times 4$ MHz for $N = 1.6 \times 10^5$ atoms) is already included in ω_c . In the non-organized phase ($\lambda < \lambda_{\text{cr}}$), the change of the dispersive cavity shift due to the small population of the motional excited state ψ_1 can be neglected for our experimental parameters (see however [S5, S4]). Working at large pump-cavity detuning, we also neglect the substructure of the atoms-shifted cavity resonance caused by the polarization dependence of the dipole transition strengths and the cavity birefringence. The coupling strength $2\lambda/\sqrt{N}$ is given by the two-photon (vacuum) Rabi frequency between pump and cavity fields [S2].

Residual driving of the cavity field due to finite-size effects of the atomic cloud [S6] and residual scattering of pump light off the cavity mirrors results in a finite coherent cavity field amplitude already in the normal phase. The presence of this field breaks the \mathbb{Z}_2 symmetry of the Dicke Hamiltonian and is modeled by the replacement $\hat{J}_x \rightarrow \hat{J}_x + \zeta$ in equation (3), where ζ (assumed to be real) determines the effective cavity drive amplitude. Effectively, ζ can be interpreted as an atomic population imbalance between even ($\cos(kx)\cos(kz) = 1$) and odd ($\cos(kx)\cos(kz) = -1$) lattice sites at zero coupling strength [S6]. Since in the experiment ζ is likely to change in sign and amplitude between different experimental runs (e.g. due to drifts of the atomic cloud center with respect to the pump-cavity mode structure), we include in the theoretical model an ensemble average according to $\zeta \rightarrow \zeta \cos(\phi)$ where ϕ is taken to change randomly between 0 and 2π .

Semi-classical steady-state solution

The self-consistent mean-field solution for $\alpha = \langle \hat{a} \rangle$, $\beta = \langle \hat{J}_- \rangle \equiv \langle \hat{J}_x - i\hat{J}_y \rangle$ and $w = \langle \hat{J}_z \rangle$ in the presence of a symmetry-breaking field ($\zeta \neq 0$) is determined from the semi-classical equations of motion of the Hamiltonian

$\hat{H} + 2\hbar\lambda/\sqrt{N}(\hat{a} + \hat{a}^\dagger)\zeta$, including cavity decay at rate κ :

$$\dot{\alpha} = -(\kappa + i\omega)\alpha - i\frac{\lambda}{\sqrt{N}}(\beta + \beta^* + 2\zeta) \quad (4)$$

$$\dot{\beta} = -i\omega_0\beta + 2i\frac{\lambda}{\sqrt{N}}(\alpha + \alpha^*)w \quad (5)$$

$$\dot{w} = i\frac{\lambda}{\sqrt{N}}(\alpha + \alpha^*)(\beta - \beta^*). \quad (6)$$

Using the conservation of \mathbf{J}^2 , i.e. $w^2 + |\beta|^2 = N^2/4$, yields the steady-state equations

$$\begin{aligned} \beta &= \frac{\lambda^2}{\lambda_{\text{cr}}^2}(\beta + \zeta)\sqrt{1 - 4\frac{\beta^2}{N^2}} \\ \alpha &= \frac{2\lambda}{i\kappa - \omega}(\beta + \zeta)/\sqrt{N}. \end{aligned} \quad (7)$$

with critical coupling strength $\lambda_{\text{cr}} = \sqrt{\frac{(\kappa^2 + \omega^2)\omega_0}{4\omega}}$, valid for $\zeta = 0$. In Fig. S1, the numerically obtained steady-state solution (α, β, w) is plotted for typical experimental parameters.

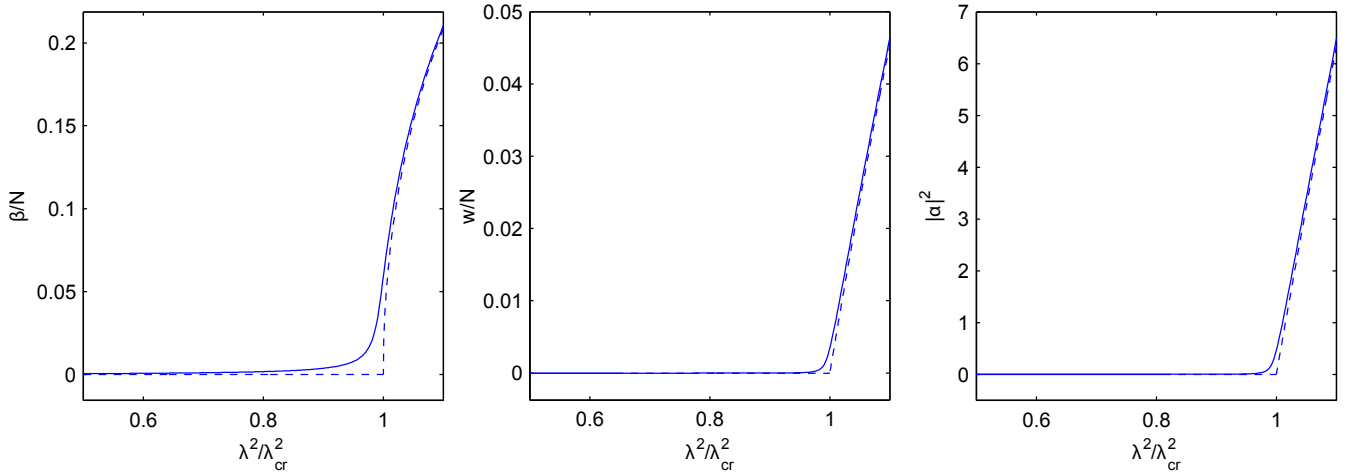


FIG. S1. Steady-state solution as a function of relative interaction strength $\lambda^2/\lambda_{\text{cr}}^2$ for our experimental parameters and an order parameter offset of $\zeta = 65$ (solid curves). The dashed curves display for comparison the case where no symmetry-breaking field is present, i.e. $\zeta = 0$ (only one branch of the bifurcation is shown). In the experiment, the intracavity photon number $|\alpha|^2$ rises much faster for $\lambda > \lambda_{\text{cr}}$ as compared to the two-mode model since the dispersive shift of the cavity frequency dynamically increases with the emerging atomic density modulation[S2].

Thermodynamic limit and quantum Langevin equations

In the thermodynamic limit, $N \gg 1$, fluctuations of the system around the semiclassical steady-state are small and can be treated in a linearized approach [S7]. This is based on the Holstein-Primakoff transformation which maps the collective spin degree of freedom $\hat{\mathbf{J}}$ to a bosonic mode with mode operators \hat{b} and \hat{b}^\dagger , defined as [S8]

$$\hat{J}_- = \hat{b}\sqrt{N - \hat{b}^\dagger\hat{b}} \quad (8)$$

$$\hat{J}_z = \hat{b}^\dagger\hat{b} - N/2. \quad (9)$$

Inserting this transformation into the Dicke Hamiltonian, Eq. (3) yields to leading order in N^{-1} the quadratic Hamiltonian

$$\hat{H}'/\hbar = \omega\delta\hat{a}^\dagger\delta\hat{a} + \tilde{\omega}_0\delta\hat{b}^\dagger\delta\hat{b} - \mu(\delta\hat{b} + \delta\hat{b}^\dagger)^2 + \tilde{\lambda}(\delta\hat{a} + \delta\hat{a}^\dagger)(\delta\hat{b} + \delta\hat{b}^\dagger) \quad (10)$$

with fluctuation operators $\delta\hat{a} = \hat{a} - \alpha$ and $\delta\hat{b} = \hat{b} - \beta/\sqrt{N}$ and renormalized parameters

$$\tilde{\omega}_0 = \omega_0 - 2\lambda \frac{\text{Re}(\alpha)\beta}{N^{3/2}\sqrt{1-\beta^2/N^2}} \quad (11)$$

$$\tilde{\lambda} = \lambda \frac{1-2\beta^2/N^2}{\sqrt{1-\beta^2/N^2}} \quad (12)$$

$$\mu = -\lambda \frac{\text{Re}(\alpha)\beta}{N^{3/2}\sqrt{1-\beta^2/N^2}}. \quad (13)$$

For our experimental parameters and $\lambda \leq \lambda_{\text{cr}}$, the maximum relative deviation of the renormalized parameters $\tilde{\omega}_0$ and $\tilde{\lambda}$ from their bare values ω_0 and λ are 0.3% and 0.7%. For simplicity, we therefore replace in the following analysis $(\tilde{\lambda}, \tilde{\omega}_0)$ by the bare values (λ, ω_0) . The squeezing term $\mu(\delta\hat{b} + \delta\hat{b}^\dagger)^2$ is also neglected in the following as $\mu/\omega_0 < 2 \times 10^{-3}$ for $\lambda \leq \lambda_{\text{cr}}$.

We model the driven-damped system dynamics with coupled quantum Langevin equations of the form [S7, S9, S10]

$$\dot{\delta\hat{a}} = -i[\delta\hat{a}, \hat{H}'] - \kappa\delta\hat{a} + \sqrt{2\kappa}\hat{a}_{\text{in}}(t) \quad (14)$$

$$\dot{\delta\hat{b}} = -i[\delta\hat{b}, \hat{H}'] - \gamma\delta\hat{b} + \sqrt{2\gamma}\hat{b}_{\text{in}}(t). \quad (15)$$

In equation (14), the bosonic operator \hat{a}_{in} describes vacuum input fluctuations of the surrounding electromagnetic field modes which are characterized by the correlation functions $\langle \hat{a}_{\text{in}}(t)\hat{a}_{\text{in}}^\dagger(t') \rangle = \delta(t-t')$ and $\langle \hat{a}_{\text{in}}^\dagger(t)\hat{a}_{\text{in}}(t') \rangle = 0$.

In contrast to [S7, S9, S10], we phenomenologically include an additional dissipation channel for the collective atomic motional degree of freedom with effective damping rate γ accompanied by atomic input fluctuations described by \hat{b}_{in} . The physical origin for this dissipation channel is attributed to collisional or cavity-mediated coupling of excitations of the momentum mode ψ_1 to Bogoliubov modes with wave vectors that are different from that of the pump and cavity fields [S11]. The collection of these modes provides a heat bath at the condensate temperature T . For simplicity, we assume this heat bath to behave Markovian. Correspondingly, we require the correlation functions for the atomic input noise in Fourier space to obey the relations

$$\langle \tilde{b}_{\text{in}}(\nu)\tilde{b}_{\text{in}}^\dagger(\nu') \rangle = 2\gamma(1+n_{\text{th}}(\nu))\delta(\nu-\nu') \quad (16)$$

$$\langle \tilde{b}_{\text{in}}^\dagger(\nu)\tilde{b}_{\text{in}}(\nu') \rangle = 2\gamma n_{\text{th}}(\nu)\delta(\nu-\nu') \quad (17)$$

with thermal mode occupation number $n_{\text{th}}(\nu) = \frac{1}{\exp(\hbar\nu/k_{\text{B}}T)-1}$. In the data analysis, the damping rate γ is taken as a free parameter which varies as a function of the relative coupling constant $\lambda/\lambda_{\text{cr}}$. This corresponds to the expectation that the density of states of the atomic heat bath, evaluated at the softening excitation frequency ω_s of the coupled system, changes when approaching the phase transition and vanishes at the critical point.

Due to the coupling between atomic and optical fields, the lowest lying excited states of the coupled BEC-cavity system acquire a finite damping rate even for $\gamma = 0$ due to a finite admixture of the cavity degree of freedom. However, the corresponding damping rate $\frac{\lambda^2}{\lambda_{\text{cr}}^2} \frac{\kappa\omega_0^2}{\kappa^2+\omega^2} < 2\pi \times 1 \text{ Hz}$ is negligible for our parameter regime, $\omega \gg \omega_0$, and does not explain the observed damping of the cavity output correlation function. Therefore we expect an additional atomic dissipation channel to be present in the system.

We solve the coupled Langevin equations (14) and (15) in Fourier space according to the conventions

$$\tilde{O}(\nu) = \frac{1}{\sqrt{2\pi}} \int_{-\infty}^{\infty} e^{i\nu t} \hat{O}(t) dt \quad (18)$$

$$\tilde{O}^\dagger(-\nu) = \frac{1}{\sqrt{2\pi}} \int_{-\infty}^{\infty} e^{i\nu t} \hat{O}^\dagger(t) dt \quad (19)$$

for any given operator \hat{O} . We thus obtain the set of coupled equations

$$\mathbf{M}(\nu) \begin{pmatrix} \delta\tilde{a}(\nu) \\ \delta\tilde{a}^\dagger(-\nu) \\ \delta\tilde{b}(\nu) \\ \delta\tilde{b}^\dagger(-\nu) \end{pmatrix} + \begin{pmatrix} \sqrt{2\kappa}\tilde{a}_{\text{in}}(\nu) \\ \sqrt{2\kappa}\tilde{a}_{\text{in}}^\dagger(-\nu) \\ \sqrt{2\gamma}\tilde{b}_{\text{in}}(\nu) \\ \sqrt{2\gamma}\tilde{b}_{\text{in}}^\dagger(-\nu) \end{pmatrix} = 0 \quad (20)$$

with the 4×4 matrix

$$\mathbf{M}(\nu) = \begin{pmatrix} -i\nu + i\omega + \kappa & 0 & i\lambda & i\lambda \\ 0 & -i\nu - i\omega + \kappa & -i\lambda & -i\lambda \\ i\lambda & i\lambda & -i\nu + i\omega_0 + \gamma & 0 \\ -i\lambda & -i\lambda & 0 & -i\nu - i\omega_0 + \gamma \end{pmatrix}.$$

We note at this point that the cavity input noise operator $\tilde{a}_{\text{in}}(\nu)$ does not vanish for negative frequencies ν in the frame rotating at the pump laser frequency ω_p . This causes the cavity environment to act e.g. on the field quadrature $\hat{a} + \hat{a}^\dagger$ effectively like a thermal bath [S12], and results in a distinct change of the fluctuation spectrum of the driven-damped Dicke model with respect to the ground state of the Dicke Hamiltonian.

The Langevin equations in Fourier space are solved by matrix inversion. Denoting the matrix elements of \mathbf{M}^{-1} by $m_{ij}(\nu)$, we obtain e.g.

$$\begin{aligned} \delta\tilde{a}(\nu) = & \sqrt{2\kappa}(m_{11}(\nu)\tilde{a}_{\text{in}}(\nu) + m_{12}(\nu)\tilde{a}_{\text{in}}^\dagger(-\nu)) \\ & + \sqrt{2\gamma}(m_{13}(\nu)\tilde{b}_{\text{in}}(\nu) + m_{14}(\nu)\tilde{b}_{\text{in}}^\dagger(-\nu)), \end{aligned} \quad (21)$$

with matrix elements

$$D \times m_{11}(\nu) = 2i\lambda^2\omega_0 - i(i\kappa + \omega + \nu)((\gamma - i\nu)^2 + \omega_0^2) \quad (22)$$

$$D \times m_{12}(\nu) = 2i\lambda^2\omega_0 \quad (23)$$

$$D \times m_{13}(\nu) = i\lambda(i\kappa + \omega + \nu)(i\gamma + \nu + \omega_0) \quad (24)$$

$$D \times m_{14}(\nu) = i\lambda(i\kappa + \omega + \nu)(i\gamma + \nu - \omega_0) \quad (25)$$

and

$$D = ((\gamma - i\nu)^2 + \omega_0^2)((\kappa - i\nu)^2 + \omega^2) - 4\lambda^2\omega\omega_0 \quad (26)$$

denoting the determinant of \mathbf{M} . Analytical expressions for the overlap integrals defined below can be obtained for our experimental parameter regime, $\omega_0 \ll \omega$, by approximating the determinant D as

$$D \simeq ((\gamma - i\nu)^2 + \omega_s^2)(\kappa^2 + \omega^2), \quad (27)$$

with the atom-like polariton frequency (soft mode frequency) defined as $\omega_s = \omega_0\sqrt{1 - \lambda^2/\lambda_{\text{cr}}^2}$ [S1]. This approximation eliminates poles of the matrix elements $m_{ij}(\nu)$ around $\nu = \pm\omega$ which do not contribute to the critical behavior of the coupled system.

According to input-output theory, the cavity output field, $\hat{a}_{\text{out}}(t)$, is given by

$$\hat{a}_{\text{out}}(t) = \sqrt{2\kappa}(\alpha + \delta\hat{a}(t)) - \hat{a}_{\text{in}}(t). \quad (28)$$

Correlation functions of the intracavity field

First-order correlation function

From (21) we obtain, using the correlation functions of the input operators,

$$\begin{aligned} \langle \tilde{a}^\dagger(\nu)\tilde{a}(\nu') \rangle = & 2\kappa|m_{12}(\nu)|^2\delta(\nu - \nu') \\ & + 2\gamma|m_{13}(\nu)|^2n_{\text{th}}(\nu)\delta(\nu - \nu') \\ & + 2\gamma|m_{14}(\nu)|^2(1 + n_{\text{th}}(-\nu))\delta(\nu - \nu') \\ & + 2\pi|\alpha|^2\delta(\nu)\delta(\nu'). \end{aligned} \quad (29)$$

In the time domain, the first-order correlation function is given by

$$G^{(1)}(\tau = t - t') \equiv \langle \hat{a}^\dagger(t)\hat{a}(t') \rangle = \frac{1}{2\pi} \int_{-\infty}^{\infty} \int_{-\infty}^{\infty} \langle \tilde{a}^\dagger(\nu)\tilde{a}(\nu') \rangle e^{i\nu t - i\nu' t'} d\nu d\nu'. \quad (30)$$

Inserting Eq. (29), this reduces to

$$G^{(1)}(\tau) = \frac{\kappa}{\pi} A(\tau) + \frac{\gamma}{\pi} \left((1 + n_{\text{th}}(\omega_s)) B(\tau) + n_{\text{th}}(\omega_s) B^*(\tau) \right) + |\alpha|^2, \quad (31)$$

where we defined overlap integrals

$$A(\tau) = \int_{-\infty}^{\infty} |m_{12}(\nu)|^2 e^{i\nu\tau} d\nu \quad (32)$$

$$B(\tau) = \int_{-\infty}^0 |m_{14}(\nu)|^2 e^{i\nu\tau} d\nu = \int_0^{\infty} |m_{13}(\nu)|^2 e^{-i\nu\tau} d\nu \quad (33)$$

and made the approximation

$$\int_{-\infty}^0 |m_{ij}(-\nu)|^2 n_{\text{th}}(\nu) d\nu \approx n_{\text{th}}(\omega_s) \int_{-\infty}^0 |m_{ij}(\nu)|^2 d\nu. \quad (34)$$

This simplification is justified by the fact that the matrix elements $m_{ij}(\nu)$ peak at $\pm\omega_s$.

Second-order correlation function

To calculate the second-order correlation function $G^{(2)}(t - t') = \langle \hat{a}^\dagger(t) \hat{a}^\dagger(t') \hat{a}(t') \hat{a}(t) \rangle$, we use the relation [S13]:

$$G^{(2)}(t - t') = |G^{(1)}(0)|^2 + |G^{(1)}(t - t')|^2 + |\langle \hat{a}(t) \hat{a}(t') \rangle|^2 - 2|\langle \hat{a}(t) \rangle|^4, \quad (35)$$

and obtain

$$G^{(2)}(\tau) = |G^{(1)}(0)|^2 + |G^{(1)}(\tau)|^2 - 2|\alpha|^4 + \left| \frac{\kappa}{\pi} C(\tau) + \frac{\gamma}{\pi} \left((1 + n_{\text{th}}(\omega_s)) D(\tau) + n_{\text{th}}(\omega_s) D^-(\tau) \right) + \xi |\alpha|^2 \right|^2 \quad (36)$$

with $\xi = \frac{(\omega - i\kappa)^2}{\kappa^2 + \omega^2}$, $D^-(\tau) = \xi B^*(\tau)$ and matrix overlaps

$$C(\tau) = \int_{-\infty}^{\infty} m_{12}(\nu) m_{11}(-\nu) e^{i\nu\tau} d\nu \quad (37)$$

$$D(\tau) = \int_{-\infty}^{\infty} m_{14}(\nu) m_{13}(-\nu) e^{i\nu\tau} d\nu. \quad (38)$$

Uncorrelated background light hitting our detector as well as detector dark counts (corresponding effectively to a mean-intracavity photon number of n_B) reduce the contrast of the oscillations in the measured second-order correlation function. To account for this, we define the normalized second-order correlation function as $g^{(2)}(\tau) = \frac{G^{(2)}(\tau) + 2|G^{(1)}(0)|n_B + n_B^2}{|G^{(1)}(0) + n_B|^2}$, which is in very good agreement with our data upon including the measured background count rate.

Determination of density fluctuations from the cavity output signal

As the lifetime of cavity photons $1/(2\kappa)$ is negligible compared to the timescale of atomic motion (determined by ω_0), we can directly infer from the detected cavity output field about the magnitude of atomic density fluctuations present in the system. The adiabatic solution of equation (14) reads

$$\delta \hat{a}(t) = \frac{\lambda(\delta \hat{b} + \delta \hat{b}^\dagger)}{i\kappa - \omega} + \sqrt{2\kappa} \int_{-\infty}^t e^{-(i\omega + \kappa)(t-t')} \hat{a}_{\text{in}}(t') dt'. \quad (39)$$

Correspondingly, the incoherent intracavity photon number $\langle \delta \hat{a}^\dagger \delta \hat{a} \rangle$ reflects directly the variance of the atomic order parameter (i.e. the variance of the checkerboard density modulation):

$$\langle \hat{J}_x^2 \rangle = \frac{N}{4} \langle (\delta \hat{b} + \delta \hat{b}^\dagger)^2 \rangle = \frac{\lambda_{\text{cr}}^2}{\lambda^2} \frac{N\omega}{\omega_0} \langle \delta \hat{a}^\dagger \delta \hat{a} \rangle \quad (40)$$

as $\langle \hat{a}_{\text{in}}^\dagger(t) \hat{a}_{\text{in}}(t) \rangle = 0$. After subtracting the coherent fraction $|\alpha|^2$ from the total detected intracavity photon number, we thus are able to extract the variance of atomic density fluctuations (Figure 5).

Comparison between experimental data and theoretical model prediction

From least-square fits of our theoretical model to the correlation data (as shown exemplarily in Figure 3C), we deduce the decay rate γ as a function of $\lambda^2/\lambda_{\text{cr}}^2$ (as shown in Figure 4) and a maximum strength of the symmetry breaking field given by $\zeta = 60(7)$. This corresponds (for $\lambda = 0$) to a finite order parameter of 0.8% relative to the maximum order parameter of $N/2 = 8 \times 10^4$. Since we observe enhanced fluctuations for $\lambda^2 > 0.97\lambda_{\text{cr}}^2$ which are not explained by our model, we deduce ζ from those correlation data where $\lambda^2 < 0.97\lambda_{\text{cr}}^2$.

We fit to the deduced γ values the empirical function $f(x) = c_1(1-x)^{c_2} \exp(c_3x) + c_4(1-x)^{c_5} \exp(c_6x)$ with $x = \lambda^2/\lambda_{\text{cr}}^2$ and free parameters c_j . The obtained functional dependence $\gamma(\lambda)$ as well as the deduced value of ζ enter the theory curves plotted in Figure 2.

In this analysis, the temperature of the atomic heat bath was set to the expected temperature $T = 100(20)$ nK of the gas after probing. This is justified by the fact that the thermal population of the momentum mode ψ_1 becomes relevant only close to the transition point due to the softening of the excitation spectrum.

Error analysis

The systematic uncertainty of the intracavity photon number (estimated to $\pm 20\%$) is dominated by the uncertainty of the detector quantum efficiency, the cavity mirror transmission and the calibration of the detector background count rate. The statistical uncertainty in the determination of $\lambda/\lambda_{\text{cr}}$ originates from power fluctuations of the transverse pump beam and residual dipole trap oscillations of the atomic cloud, which convert into fluctuations of the critical pump power. The uncertainty of ζ converts into an uncertainty of the deduced atomic density fluctuations $\langle(\hat{b} + \hat{b}^\dagger)^2\rangle$, as indicated by the errorbars in Figure 5.

* Email: donner@phys.ethz.ch

- [S1] R. Mottl, F. Brennecke, K. Baumann, R. Landig, T. Donner, and T. Esslinger. Roton-Type Mode Softening in a Quantum Gas with Cavity-Mediated Long-Range Interactions. *Science*, 336(6088):1570–1573, June 2012.
- [S2] K. Baumann, C. Guerlin, F. Brennecke, and T. Esslinger. Dicke quantum phase transition with a superfluid gas in an optical cavity. *Nature*, 464(7293):1301–1306, April 2010.
- [S3] D. Nagy, G. Kónya, G. Szirmai, and P. Domokos. Dicke-Model Phase Transition in the Quantum Motion of a Bose-Einstein Condensate in an Optical Cavity. *Physical Review Letters*, 104(13):130401+, Apr 2010.
- [S4] M. J. Bhaseen, J. Mayoh, B. D. Simons, and J. Keeling. Dynamics of nonequilibrium Dicke models. *Physical Review A*, 85:013817+, January 2012.
- [S5] J. Keeling, J. Bhaseen, and B. Simons. Liquid-crystalline phases of ultracold atoms. *Physics*, 3:88, Oct 2010.
- [S6] K. Baumann, R. Mottl, F. Brennecke, and T. Esslinger. Exploring Symmetry Breaking at the Dicke Quantum Phase Transition. *Phys. Rev. Lett.*, 107(14):140402, September 2011.
- [S7] F. Dimer, B. Estienne, A. S. Parkins, and H. J. Carmichael. Proposed realization of the Dicke-model quantum phase transition in an optical cavity QED system. *Phys. Rev. A*, 75(1):013804–14, January 2007.
- [S8] N. Lambert, C. Emery, and T. Brandes. Entanglement and the Phase Transition in Single-Mode Superradiance. *Physical Review Letters*, 92(7):073602+, February 2004.
- [S9] D. Nagy, G. Szirmai, and P. Domokos. Critical exponent of a quantum-noise-driven phase transition: The open-system Dicke model. *Physical Review A*, 84:043637+, October 2011.
- [S10] B. Öztürk, M. Bordyuh, Ö. E. Müstecaplıoglu, and H. E. Türeci. Excitations of optically driven atomic condensate in a cavity: theory of photodetection measurements. *New Journal of Physics*, 14(8):085011, 2012.
- [S11] R. Graham. Langevin Equation of Collective Modes of Bose-Einstein Condensates in Traps. *Journal of Statistical Physics*, 101(1):243–257, 2000.
- [S12] E. Dalla Torre, S. Diehl, M. Lukin, S. Sachdev, and P. Strack. Keldysh approach for nonequilibrium phase transitions in quantum optics: Beyond the Dicke model in optical cavities. *Phys. Rev. A*, 87(2):023831, February 2013.
- [S13] M. Naraschewski and R. J. Glauber. Spatial coherence and density correlations of trapped Bose gases. *Phys. Rev. A*, 59(6):4595–4607, June 1999.